Available online at www.sciencedirect.com
SCIENCE DIRECT®
Journal of Nuclear Materials 354 (2006) 1–13
journal of nuclear materials
www.elsevier.com/locate/jnucmat

Irradiation stability of R7T7-type borosilicate glass

S. Peuget *, J.-N. Cachia, C. Jégou, X. Deschanels, D. Roudil, V. Broudic, J.M. Delaye, J.-M. Bart

Commissariat à l'Énergie Atomique (CEA), Rhône Valley Research Center, BP 17171, 30207 Bagnols-sur-Cèze cedex, France

Received 16 May 2005; accepted 13 January 2006

Abstract

High-level nuclear waste containment glass is subjected to irradiation-induced stresses whose consequences must be assessed to guarantee the material behavior over time. Alpha decay from the minor actinides confined in the glass structure is responsible for most of the atom displacements. Minor actinide concentrations in the glass exceeding current levels are under consideration for future vitrification scenarios. Four R7T7-type borosilicate glass samples doped with 0.04, 0.4, 1.2 and 3.25 wt% $^{244}CmO_2$ were fabricated to study not only the cumulative effect of high alpha decay doses ($>10^{19}$ α/g) but also of the dose rate. The homogeneity of the materials and their chemical compositions were characterized to ensure they were suitably representative for the experimental program. The macroscopic behavior of the glasses was characterized for doses up to 3×10^{18} α/g. No significant effect on the initial alteration rate was detected which means that the chemical reactivity of the glass with pure water is not affected by such levels of alpha doses. The glass swelled slightly depending on the dose, saturating at about 0.5% after receiving a dose of about 2×10^{18} alpha disintegrations per gram of glass. The mechanical properties were observed to improve appreciably, with lower hardness but greater fracture toughness. A stabilization phenomenon comparable to that of the glass density was also observed. Comparing the experimental data with other findings obtained by atomistic modeling and external irradiation suggests that nuclear interactions caused by alpha decay recoil nuclei could be responsible for the experimental variations observed. The possible origins of the observed variations in macroscopic properties are also discussed.

PACS: 28.41.Kw; 61.43.Fs; 81.05.Kf

1. Introduction

Fission products and minor actinides are currently stabilized and immobilized by vitrification in France; this is the French reference process for industrial management of such high-level wasteforms. 'R7T7' glass, named after the COGEMA La Hague vitrification units, is the reference glass selected to immobilize the radioelements arising from reprocessing light-water reactor fuel. Developments in the characteristics – and notably the burnup – of the fuel used in nuclear power plants modify the isotopic composition of the radioactive elements to be immobilized. Depending on the glass loading factor, this could

* Corresponding author. Tel.: +33 466 796529; fax: +33 466 797708.
E-mail address: sylvain.peuget@cea.fr (S. Peuget).

0022-3115/$ - see front matter © 2006 Elsevier B.V. All rights reserved.
doi:10.1016/j.jnucmat.2006.01.021

result in a higher concentration of minor actinides in the glass, and thus an increase in the cumulative alpha decay sustained by the material.

The effect of alpha decay on the containment properties of sodium borosilicate nuclear glass can be assessed by doping the glass with short-lived actinides (^{242}Cm, ^{244}Cm, ^{238}Pu); only a few years are necessary to reach doses equivalent to those sustained by the glass several thousand years after disposal. The effects of alpha decay on the macroscopic properties of different glass compositions have been documented in the literature for doses of up to 5×10^{18} alpha disintegrations per gram of glass [1–7]. To the best of our knowledge, however, only a few studies have addressed particular aspects of nuclear glass behavior when subjected to higher integrated doses [3,8,9]. The data have been summarized in surveys of the irradiation behavior of vitreous materials [10–12]. In order to assess the behavior of R7T7-type glass at integrated doses above 10^{19} α/g, an experimental research program involving the fabrication and characterization of curium-doped glass samples was initiated in 2001 in the CEA's Atalante-DHA facility at Marcoule.

This article describes the conditions under which the materials were fabricated and initially characterized to ensure their suitability for the experimental program. Moreover, the results of the macroscopic property measurements versus the alpha decay dose in the range described up to now by these glasses are shown and discussed in the light of published data concerning irradiation effects in silicate glasses.

2. Material

2.1. Fabrication

Four glass samples doped with 0.04, 0.4, 1.2 and 3.25 wt% $^{244}CmO_2$ were fabricated to investigate the effect of the integrated dose and of the dose rate on the glass behavior.

In the test glasses, fission products were simulated by their stable isotopes or by chemical elements having similar behavior. For the specimens doped with 0.04, 0.4 or 1.2 wt% $^{244}CmO_2$, the added curium was offset by proportionally diminishing the concentrations of all the other glass constituents. A different approach was adopted for the specimen doped with 3.25 wt% $^{244}CmO_2$, considering the isotopic composition of the curium used (Table 1) and the high target concentration. In the absence of quantitative data on the cumulative actinide and lanthanide loading limits in this glass composition, the quantity of lanthanides at oxidation state +III was intentionally diminished to limit the risk of precipitation of secondary phases containing curium. Considering the equivalent structural roles of the actinides and lanthanides in this type of glass [13,14], the composition changes resulting from the higher curium concentration were not expected to have any significant consequences on the material properties. The theoretical chemical compositions of the two glasses with the highest doped curium content are shown in Table 2.

The glass samples were produced by melting oxides, carbonates and nitrates. The first step, prior to initiating each glass melt, consisted in dissolving curium oxide in a 3 mol L^{-1} nitric acid solution and measuring the Cm concentration by isothermal calorimetry in order to adjust the solution volume to obtain the desired concentration in the glass. The curium-doped nitric acid solution was then

Table 1
Isotopic composition of curium used for glass fabrication (June 30, 2004)

Isotope	^{243}Cm	^{244}Cm	^{245}Cm	^{246}Cm	^{247}Cm	^{248}Cm
Atomic %	0.84%	78.82%	9.61%	9.82%	0.47%	0.43%

Table 2
Chemical composition (wt%) of glass rods doped with 1.2 wt% and 3.25 wt% $^{244}CmO_2$

Shared basic composition						Sample-specific composition changes		
SiO_2	45.28	Cr_2O_3	0.52	BaO	0.61	Y_2O_3	0.2	0
B_2O_3	13.97	ZnO	2.5	Ag_2O	0.03	La_2O_3	0.92	0.92
Na_2O	10.1	P_2O_5	0.29	CdO	0.03	Ce_2O_3	0.95	0
Al_2O_3	4.94	SrO	0.34	SnO_2	0.02	Nd_2O_3	1.64	0
CaO	4.02	ZrO_2	2.72	TeO_2	0.23	Pr_2O_3	0.45	0
Li_2O	1.97	MoO_3	1.76			$^{240}PuO_2$	0.12	0.74
Fe_2O_3	2.99	MnO_2	0.38			CmO_2	1.5	4.12
NiO	0.42	Cs_2O	1.1			(Incl. $^{244}CmO_2$)	1.2	3.25

added to the oxides in a platinum crucible. This method was selected rather than a dry route to favor curium solubilization in the glass. The mixture was melted for 3 h at 1200 °C without stirring, then quenched to a temperature slightly above the glass transition point (600 °C), from which it was cooled more slowly to release the residual stresses from the glass. Fig. 1 is a photo of the crucible containing the glass doped with 1.2 wt% $^{244}CmO_2$. The cylindrical glass rods measured 15 or 20 mm in diameter and weighed between 30 and 100 g.

2.2. Characterization methods

Fig. 2 identifies the characterization specimens taken from the rods for chemical composition and homogeneity analysis. The glass rods were first analyzed lengthwise by gamma spectrometry on the ^{243}Cm lines (228.18 and 277.6 keV) to estimate the homogeneity of the axial curium distribution. A curium concentration profile was also obtained with a Cameca SX50 electron microprobe on a specimen taken from the bottom of the glass rod doped to 3.25 wt% to confirm the gamma spectrometry results.

The rods were cut into disks, and representative samples of the top, center and bottom of each rod were examined to determine their microstructural homogeneity and chemical composition.

Possible secondary phases were detected by a combination of optical microscopy, scanning electron microscopy. X-ray diffraction analysis was also used to determine the presence of crystalline secondary phases. The examination was carried out using a Seifert diffractometer in Bragg–Brentano geometry (2θ range: 5–80°, step 0.02°, time 10 s/step). The source corresponds to Kα line of copper; a monochromator was used to eliminate Kβ lines.

The chemical composition of the glass was determined after hot acid dissolution of the specimens: elemental chemical analysis by ICP-AES for the nonradioactive elements, and radiochemical analysis for curium. The ^{244}Cm concentration in the glass was also determined by isothermal calorimetry by measuring the heat power generated by the glass samples.

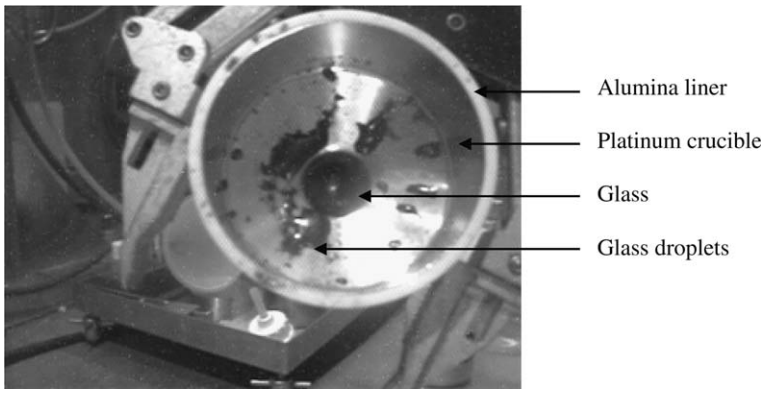

Fig. 1. Photo of the crucible containing the glass doped with 1.2 wt% $^{244}CmO_2$.

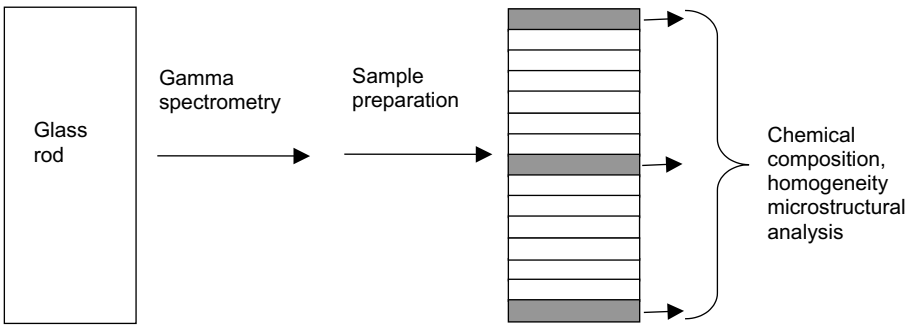

Fig. 2. Glass rod characterization specimens.

2.3. Curium distribution in the glass rods

The radial curium distribution was determined by electron microprobe analysis to obtain a curium concentration profile between the center and the edge of the rod. Only qualitative analysis was possible for lack of a curium measurement standard. The results indicated a uniform radial curium distribution between the center and the outer edge of the rod.

Fig. 3, showing the longitudinal curium distribution determined by gamma spectrometry and electron microprobe examination of the glass specimens doped to 1.2 and 3.25 wt% $^{244}CmO_2$, reveals an enrichment zone in the last few millimeters at the bottom of the rod; the amplitude differs according to the glass, i.e. 15% for the 1.2% doped specimen versus 30% for the 3.25% doped specimen. This is probably related to curium accumulation by gravity in the molten glass. However, the comparable height of the enrichment zone in all the glass rods suggests that this accumulation is probably due to inadequate convection at the bottom of the small-diameter (15 and 20 mm) crucibles. The amplitude of the phenomenon appears to depend on the overall height of the glass: the smallest amplitude was observed in the longer rods, as the enrichment at the bottom of the rod was spread over a longer zone.

This result shows the importance of characterizing the longitudinal curium distribution in order to estimate the actual dose received by the specimens sampled from the rods. The bottom portion of these glass rods will thus receive cumulative doses up to 30% higher over the same time period.

2.4. Material homogeneity

Fig. 4 shows optical and scanning electron microscopic images of the glass doped with 1.2 wt% $^{244}CmO_2$. The microstructure of all the glass samples was homogeneous at these scales, with no secondary crystalline phases. The X-ray diffraction analysis performed tends to confirm this point because of the absence of diffraction peaks (Fig. 5). We must mention that, due to the size of the beam, the XRD pattern takes into account the glass contribution but also the contribution of the resin in which the glass is embedded.

2.5. Chemical composition

The chemical composition of the glass samples doped with 0.04, 0.4, and 1.2 wt% $^{244}CmO_2$ was determined, after dissolving the glass specimens, by ICP-AES elemental chemical analysis for the nonradioactive elements and by radiochemical analysis for curium. The ^{244}Cm concentration was also determined by isothermal calorimetry in the solid samples prior to dissolution.

Table 3 compares the experimental concentrations of the major glass constituent oxides with the theoretical values determined from the mass of each constituent used in elaboration process. The satisfactory agreement validates the experimental protocol. To avoid diminishing the quantity of 3.25 wt% $^{244}CmO_2$-doped glass available for characterization, we considered that chemical analysis following hot dissolution was unnecessary. Only the curium concentration was determined by isothermal calorimetry, yielding a concentration of 3 wt%

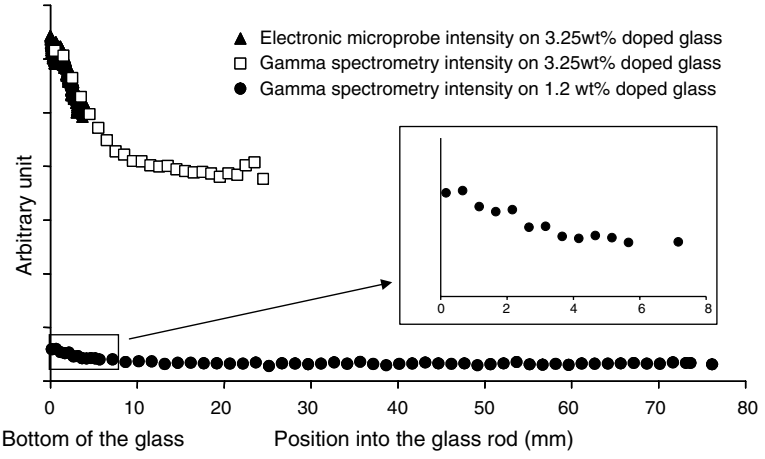

Fig. 3. Longitudinal curium distribution in glass rods doped with 1.2 wt% and 3.25 wt% $^{244}CmO_2$.

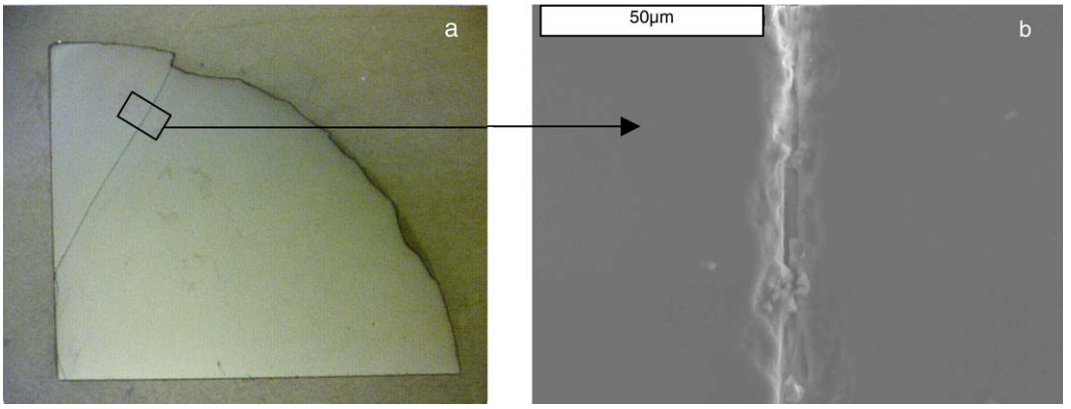

Fig. 4. Photos of a glass specimen doped with 1.2 wt% $^{244}CmO_2$: (a) optical microscope (×10), (b) scanning electron microscope.

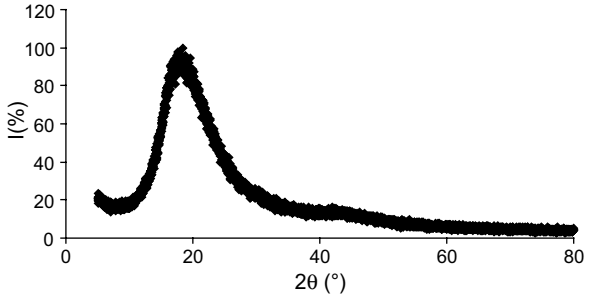

Fig. 5. XRD pattern of a glass specimen doped with 1.2 wt% $^{244}CmO_2$.

$^{244}CmO_2$ in the zone of constant curium concentration.

Together with the gamma scanning results on the glass rods, quantitative curium concentration analysis was thus able to accurately determine the curium concentration of each specimen sampled from the various rods. In the 1.2 and 3.25 wt% doped glass rods, the concentrations determined in the constant concentration zone were 1.2 and 3 wt% $^{244}CmO_2$, respectively, and 1.38 and 4 wt% $^{244}CmO_2$ at the bottom of the rod.

3. Characterization of macroscopic properties versus dose

3.1. Characterization methods

3.1.1. Leach rate measurement

The initial glass alteration rates, which reflect the chemical reactivity between the glass matrix and pure water, were determined by Soxhlet-mode dynamic leach testing at 100 °C. A specimen disk (21 mm in diameter and 2 mm thick) was placed in an overflowing sample holder designed to ensure contact between the glass and continuously renewed pure water. Solution samples were taken at regular intervals during the 28-day test for ICP-AES and radiochemical analysis. The initial glass alteration rate was determined by monitoring the release of glass alteration tracer elements (B, Na, Li, Mo) and by measuring the sample weight loss.

3.1.2. Density measurement

The density of the curium-doped glass was measured by means of a hydrostatic balance; the glass sample was weighed in air, then in water

Table 3
Chemical composition analysis results for glass samples doped with 0.04, 0.4 and 1.2 wt% $^{244}CmO_2$ (major oxides)

$^{244}CmO_2$		SiO_2	B_2O_3	Na_2O	Al_2O_3	CaO	CmO_2 (radiochemistry)	CmO_2 (calorimetry)
0.04 wt%	Experimental	49.1 ± 3.1	14.1 ± 0.9	10.8 ± 0.3	5.1 ± 0.6	3.9 ± 0.3	0.045 ± 0.008	0.044 ± 0.004
	Theoretical	46	14.2	10.3	5.0	4.1	0.043	0.043
0.4 wt%	Experimental	48.8 ± 3.8	15.1 ± 0.6	9.9 ± 0.6	5.6 ± 0.7	4.1 ± 0.4	0.36 ± 0.06	0.42 ± 0.02
	Theoretical	45.8	14.3	10.3	5.0	4.1	0.43	0.43
1.2 wt%	Experimental	46.5 ± 3.7	14.1 ± 0.7	9.9 ± 0.2	4.7 ± 1.4	3.6 ± 0.9	1.17 ± 0.21	1.2 ± 0.06
	Theoretical	45.3	14.0	10.1	4.9	4.0	1.2	1.2

according to Archimedes' principle. The sample density represents the mean value of ten measurements.

3.1.3. Hardness measurement

The glass hardness was measured in air by Vickers micro-indentation on polished specimens, with indenter loads of 200 g maintained for 20 s. The Vickers hardness was determined from the length of the diagonals of the indentation according to Eq. (1).

$$H_V = \frac{2F\sin\left(\frac{\theta}{2}\right)}{d^2}, \quad (1)$$

where H_v is the Vickers hardness, F the force applied, θ the angle between the opposite pyramid faces and d is the mean length of the indentation diagonal. For each characterization, the hardness represents the mean value of ten indentation tests.

3.1.4. Young's modulus measurement

The reduced Young's modulus of the glass was determined by biaxial flexure. A cylindrical glass test piece (2 mm thick and 21 mm in diameter) supported on three balls 120° apart was subjected to a force centrally applied by a piezoelectric device. The stress load was measured by a force sensor and the strain was observed on the sample by means of a scattered light interferometry technique. The reduced Young's modulus was determined from the force applied and the sample deflection by using Eq. (2).

$$\frac{E}{(1-\upsilon^2)} = \frac{\alpha \times r^2 \times F}{D \times e^3}, \quad (2)$$

where E is Young's modulus, υ Poisson's coefficient, α a factor related to the number of bearing points, r the supporting ball radius, F the force applied to the sample, D the deflection and e the sample thickness.

The four curium-doped glass samples were characterized as above at the earliest possible moment after fabrication in order to measure the glass reference properties before any significant cumulative alpha decay occurred. The samples were then characterized at regular intervals to monitor the variations in these properties versus the cumulative alpha decay.

3.2. Initial alteration rate

Fig. 6 shows the initial alteration rate of the curium-doped glass samples versus the cumulative alpha decay. The indicated experimental uncertainty was determined from the uncertainty on each steps in the process of calculating the initial alteration rate, i.e. estimating the reactive surface area of the pellet, chemical analysis of the element concentrations in solution, and weighing out the sample volumes.

The measurements of the three glass samples doped to 0.04, 0.4 and 1.2 wt% do not show significant variations: the data points are all comparable within the experimental uncertainty. Most published findings are based on rates determined from sample mass losses (by weighing before and after leaching), which can underestimate the actual alteration rate because of the formation of an alteration film (Table 4). The rates indicated here were deter-

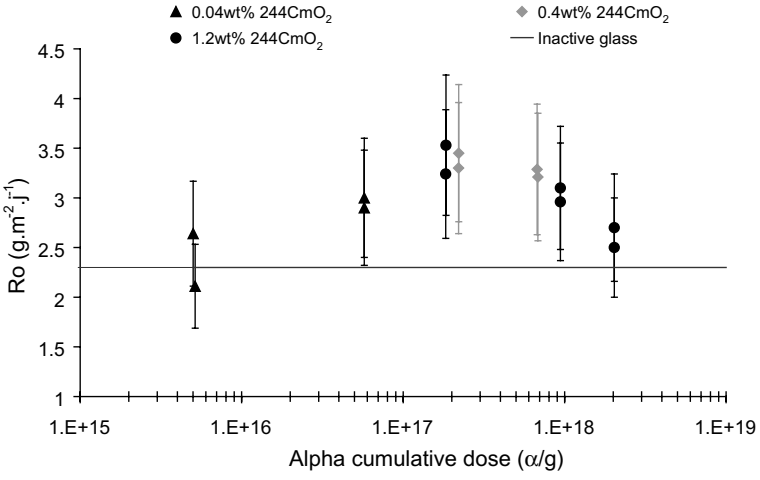

Fig. 6. Initial alteration rate Ro, based on measured release of tracer elements (Na, B, Li, Mo), versus cumulative alpha decay in curium-doped glasses.

Table 4
Initial alteration rate, based on sample masse losses and on the release in solution of tracer elements (Na, B, Li, Mo), versus cumulative alpha decay in curium-doped glasses

Cumulative alpha decay (α/g)	5×10^{15}	6×10^{16}	2×10^{17}	2×10^{17}	7×10^{17}	2×10^{18}
Concentration of $^{244}CmO_2$ (%)	0.04	0.04	0.4	1.2	0.4	1.2
Ro from sample masse losses (g/m ^{2}/J)	2.04	2.33	2.58	2.53	2.44	2.35
Ro from the release of tracer elements (g/m ^{2}/J)	2.38	2.95	3.37	3.4	3.25	2.6

mined from the release into solution of glass alteration tracer elements. These results clearly show that cumulative alpha decay up to doses of 2×10^{18} α/g does not increase the initial rate alteration by more than the measurement uncertainty, i.e. 20%. These findings are also consistent with the results recently reported by Wellman et al. [15] for plutonium-doped glass over a comparable dose range.

These results show that the initial alteration rate is not significantly affected by the accumulation of alpha decay in the glass; the initial rate after 2×10^{18} α/g is equivalent to that of an inactive glass with the same composition. It is interesting to notice that industrial glasses will have cumulated an alpha dose around 3×10^{18} α/g when water is supposed to access to the glass in storage conditions.

3.3. Density

The density (Fig. 7) diminished as a function of the cumulative alpha dose of the three curium-doped glass specimens, reaching 0.4–0.5% after 2×10^{18} α/g for the samples doped with 1.2 and 3.25 wt% $^{244}CmO_2$. The slight swelling of the glass with the alpha decay dose is consistent with the behavior observed by Matzke [6] in glass of a similar chemical composition doped with 1.5 wt% curium: glass swelling by 0.5 to 0.6% was observed after 2×10^{18}α/g. The overall results obtained for glass samples doped with 0.4, and 1.2 and 3.25 wt% $^{244}CmO_2$ are in good agreement and appear to follow the same curve, suggesting that the dose rate has no effect on this property within the range studied.

The slight glass swelling arising from irradiation appeared to stabilize after a dose of about 2×10^{18}α/g, which is also in agreement with published findings [12].

3.4. Hardness

Fig. 8 shows the hardness variation for the four doped glass specimens versus the cumulative alpha decay. Only a single data point is shown for the glass doped to 0.04 wt% because no variation was observed up to 10^{17} α/g. The decrease in the material hardness, which reached about 30–35% after a dose of 1.5×10^{18} α/g, was equivalent for the glass samples doped with 0.4, 1.2 and 3.25 wt%

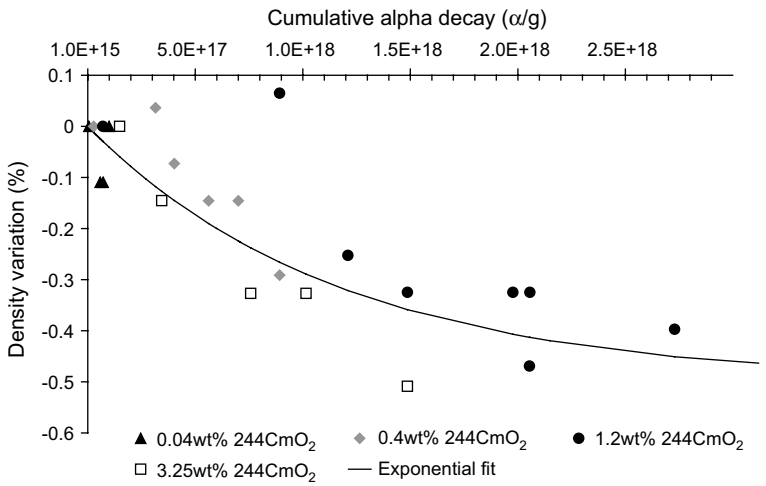

Fig. 7. Density versus cumulative alpha decay in curium-doped glasses.

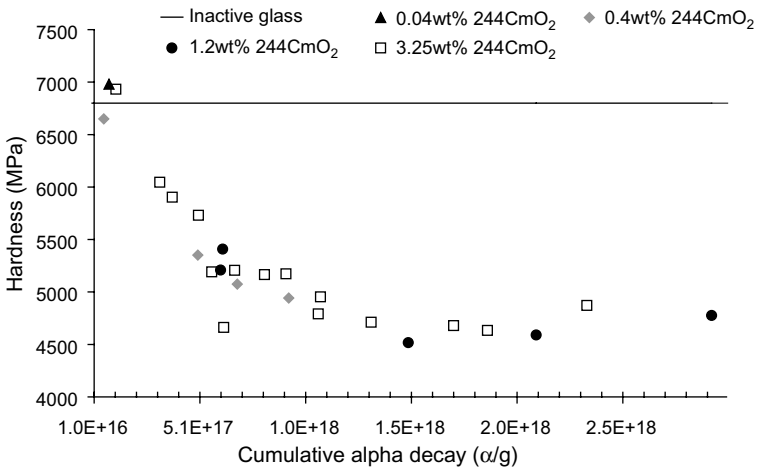

Fig. 8. Hardness versus cumulative alpha decay in curium-doped glasses.

$^{244}CmO_2$, again indicating the absence of any dose rate effect within the range studied here. The hardness was observed to stabilize above this dose. The plastic response of the glass to an indentation test is accentuated by the effect of alpha decay on the glass structure. This is consistent with the behavior reported in the literature for identical doses and summarized by Weber [12], and with the experimental results of external irradiation of R7T7-type glass by heavy ions [16,17].

In addition to these variations, it is interesting to note that the occurrence probability of cracks at the corners of the hardness indentation also diminished with the dose from about 80% under a 300 g load for a dose of 5×10^{16} α/g, to 50% after 6×10^{17} α/g, and to zero above 10^{18} α/g. This behavior reflects the increase in the glass fracture toughness with damage, and was also reported by Matzke [6] and Inagaki [9] during fracture toughness measurements by indentation.

3.5. Reduced Young's modulus

Fig. 9 shows the reduced Young's modulus of the doped glass specimens. Difficulties related to the equipment setup prevented characterization of the elastic modulus of the 0.4 and 1.2 wt% doped glass samples before they had reached doses of 4 and 7.5×10^{17} α/g, respectively. In view of the dose-dependent density and hardness variations described above, it would be unwise to consider these values as representative of the initial glass properties.

For the glasses doped with 0.04, 0.4 and 1.2 wt% $^{244}CmO_2$ it is difficult to identify any variation in the

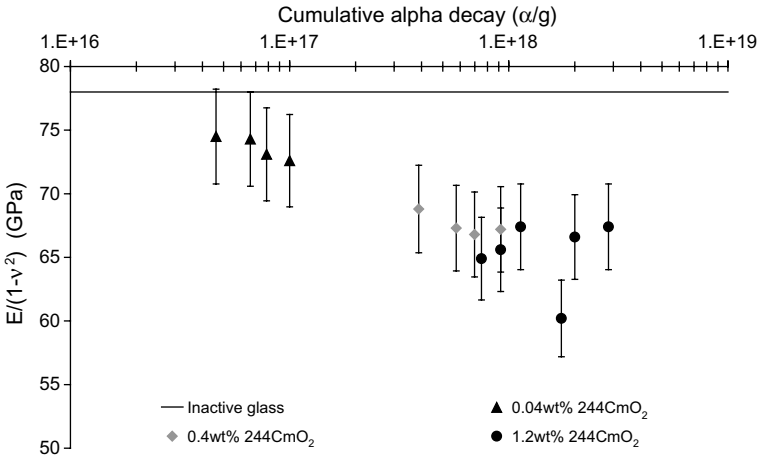

Fig. 9. Reduced Young's modulus versus cumulative alpha decay in curium-doped glasses.

reduced Young's modulus versus the cumulative alpha decay over the dose range investigated. Considering the error margins, the data suggest that the reduced modulus did not vary with the damage, but rather that the initial values differed from one glass sample to another.

Nevertheless, a comparison of the data for the 0.04 and 0.4 wt% doped glass suggests that the modulus diminished by about 15% between 6×10^{16} and 6×10^{17} α/g, as shown by the declining trend of the curve over the last few data points for the 0.04 wt% sample and the slight decrease over the first few points for the 0.4 wt% sample.

Measurement data between 10^{17} and 4×10^{17} α/g will be necessary to decide between the two hypotheses. However, published reports concerning this type of glass indicate a decrease in the modulus of elasticity by approximately 30% after about 10^{18} α/g [9,18], which is not compatible with the results of this study, although the experimental technique used in those studies differed from the method used here. A more detailed study of the influence of the methodology used must be undertaken to clear up this issue.

4. Discussion about the evolution of the macroscopic properties

4.1. Density

The density variation described by the points in Fig. 7 resembles an exponential function. We therefore chose to apply Marples' model [5], in which the sample volume variation is proportional to the damaged volume fraction in the material. The density variation is thus described by the following relation:

$$\frac{\Delta\rho}{\rho_0} = A\left(1 - e^{-\rho_0 VD}\right), \tag{3}$$

where ρ is the glass density, A the maximum density variation (%), D the cumulative alpha decay (α/g) and V is the glass volume damaged per alpha disintegration.

The results of the fit are also shown in Fig. 7, with a density variation that saturates at −0.5%, and a damage volume of 310 nm^3 per alpha disintegration. Considering the number of measurements and their dispersion, a satisfactory fit can be obtained for the experimental data by varying the A and V parameters from −0.48 to −0.59% and from 190 to 350 nm^3, respectively.

It is interesting to compare these results with those obtained by numerical modeling of the deceleration of a recoil nucleus in a simplified borosilicate glass. A type of molecular dynamics taking only ballistic collisions into account has recently been developed to predict the morphology of displacement cascades at energies ranging from 0 up to 80 keV. This method is described in detail in Ref. [19]. It has been validated for the projectile path length and number of atom displacements compared with classical molecular dynamics, and with the TRIM code. It is thus possible to simulate the positions of all the atoms subjected to a collision during a displacement cascade. Fig. 10 shows a typical cascade initiated by a 70 keV projectile. Branching subcascades are visible around the main projectile track. Defining the effective volume of a cascade is thus an elusive problem because it is difficult to delimit precisely the space concerned by the atomic displacements. We have nevertheless attempted to bound the cascade volume using the following technique: a mesh of elementary cells with a definite unit volume is applied to the simulation cell containing 8×10^6 atoms and the cascade volume is defined as the set of unit cells containing at least one atom displacement. This method provides a conservative value for the cascade volume. Fig. 11 shows the cascade volume variation versus the incident projectile energy: a virtually linear increase can be observed between 0 and 80 keV. Extrapolating this trend to 97 keV (the energy of ^{240}Pu nuclei

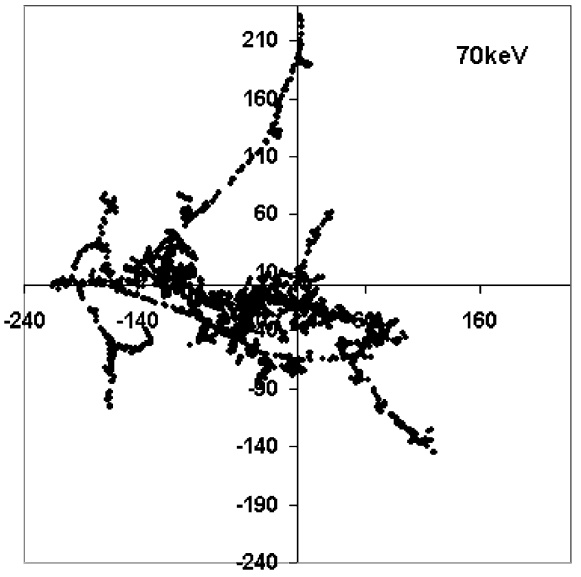

Fig. 10. Morphology of a cascade initiated by a 70 keV recoil nucleus (only atoms affected by collisions are shown).

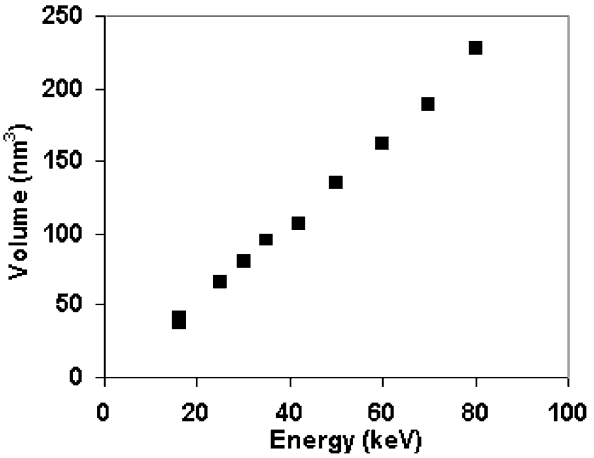

Fig. 11. Cascade volume variation versus incident projectile energy.

arising from ^{244}Cm decay) yields a volume of about 270 nm^3 per cascade.

The correlation between the volume of a simulated cascade and the value given by applying Marples' model to the experimental data points suggests that swelling is related to the damage generated by the passage of the recoil nucleus in the glass matrix.

Moreover, glass damage analysis using Marples' model also shows that the density variation stabilizes when the entire material volume has been damaged by nuclei recoil. The absence of further density variations at higher doses could imply that a second recoil nucleus passing through a previously damaged zone has no additional effect on this parameter. In the absence of any other potential source of density modifications, this suggests that the density would remain stable thereafter.

It is possible, however, that helium generated within a material can result in significant macroscopic swelling, as observed with absorbent ceramics such as B_4C and HfB_2 [20]. This appears to be the mechanism chosen by Inagaki to account for most of the glass swelling under alpha self-irradiation [8]. Inagaki, working with curium-doped glass that had received a cumulative dose of 10^{19} α/g, noted that the density and size of bubbles in this glass could account for the 0.5% swelling observed with another doped glass of the same composition after 6×10^{18} α/g [8]. This reasoning appears to be supported by the correlation between the macroscopic swelling recovery at high temperatures and the bubble size and density variations following high-temperature annealing, observed differently in these two curium-doped glass samples.

A more comprehensive discussion of experimental observations in the literature is required to assess the possibility that the swelling observed in curium-doped glass can be attributed to the formation of helium bubbles. Assuming the swelling is due to the creation of helium bubbles in the material, the saturation observed between 2 and 6×10^{18} α/g would imply that the glass microstructure stabilizes; this supposes that the helium produced within this range is released from the sample. The stabilization phenomenon thus includes a kinetic aspect, and in this respect the published observations of density stabilization at about 2×10^{18} α/g irrespective of the dose rate, sample size and irradiation conditions (doped glass [12], in-pile irradiation [21]) are somewhat surprising.

Moreover, several types of behavior under alpha self-irradiation are reported depending on the chemical composition: the glass may exhibit either swelling or densification [12]. American 72–68 glass samples, which were subject to about 1% densification after 2×10^{18} α/g [3], still contained all the helium generated [22,23]. In-pile irradiation studies based on the ^{10}B(n,α)^{7}Li [21] nuclear reaction to simulate alpha decay effects revealed pores 0.2 μm in diameter, suggesting the presence of helium bubbles. However, the pores are observed in glass samples whether subject to swelling or densification.

It is thus difficult to attribute the density variations observed up to 2×10^{18} α/g in the various nuclear glasses studied to the formation of helium bubbles alone. It is more likely that the density changes are the consequence of structural changes resulting from electronic and nuclear interactions by alpha particles and recoil nuclei: the preceding analysis of the damage volumes would tend to emphasize ballistic effects.

4.2. Mechanical properties

This study revealed an increase in the plastic response of the glass, as well as its resistance to cracking. It is interesting to discuss these mechanical property variations with regard to the glass brittleness, defined by Lawn and Marshall [24] as the ratio between the hardness and the fracture toughness $B = H_v/K_c$. The less brittle the glass, the more readily it deforms and the more difficult it is to fracture. The lower hardness and greater fracture toughness of irradiated nuclear glasses thus reflect decreasing brittleness, which diminishes from 8 to 4 $\mu m^{-1/2}$ (calculated from the data of this study and the

results of Matzke [18]) between the initial and irradiated glass, after stabilization of the macroscopic properties. Several explanations have been proposed to account for changes in glass brittleness, and in particular for the increased fracture toughness, e.g. the presence of bubbles [9] in the glass structure could enhance its crack propagation resistance, or external compression of recoil nuclei tracks [18] could locally strengthen the material. The decreasing brittleness could also result from increased plastic deformation at the root of cracks in the glass [25]. An approach similar to the one adopted by Ito [26] concerning the brittleness of aluminosilicate glass can also be applied here. Ito uses the following relation between the deformation zone R at the crack root and the glass brittleness glass B:

$$R = \frac{\pi}{8}\left(\frac{\alpha}{B}\right)^2, \tag{4}$$

where α is a constant between 1.6 and 1.9 for most glasses. This expression shows that the least brittle glasses exhibit the greatest deformation because they facilitate mechanical stress relaxation near the crack roots. The structure of nuclear glasses modified by irradiation could thus be more readily deformable, resulting in a less brittle material.

5. Origin of the observed variations in macroscopic properties

5.1. Effect of recoil nuclei and alpha particles

The preceding discussion implies that the evolution of the density and mechanical properties arises from structural changes due to alpha decay. It is interesting in this context to mention the results of external irradiation of inactive surrogate glass samples by heavy ions [16,17] resulting in identical hardness variations for externally irradiated glass and for curium-doped glass, considering the nuclear energy deposited in the material. This suggests that the recoil nuclei – the main contributors to the nuclear energy transferred – are responsible for the property variations. This assumption is supported by electron irradiation results with R7T7-type glass [27]; no appreciable macroscopic swelling ($<0.02\%$) or changes in mechanical properties were detected for a dose of 2×10^9 Gy, which corresponds to the electronic energy deposited by about 3×10^{18} α disintegrations per gram. All these studies thus indicate that the alpha decay recoil nucleus, through elastic interactions with the atoms in the glass, is responsible for the changes in density and mechanical properties observed as a function of the cumulative alpha decay.

5.2. Consequence of ballistic effects on the glass structure

Few studies are available concerning the effect of deposited nuclear energy on structural changes in silica oxide glass subjected to irradiation. Simon, Primak and Bates [28–30] showed that the roughly 3% densification of silica glass after neutron irradiation is attributable to structural reorganization of the silicate network, as demonstrated by the decreasing angles between SiO_4 tetrahedra and an increasing population of 3-member rings [31]. Similar changes in fused silica are also observed after irradiation by electrons [32], but the effectiveness of the ballistic processes is at least 200 times greater [12]. An EXAFS study of actinide-doped borosilicate glass by Hess and Weber [33] revealed few short-range modifications, although the environment around the network modifiers was more affected than that of the network formers. A slight decrease in the cation-Si distance was noted after a cumulative dose of 1.9×10^{18} α/g, suggesting a structural modification of the silicate network corresponding to a change in the Si–O–Si angle. More recently, after irradiating borosilicate glass by heavy ions to investigate the effect of the deposited nuclear energy, Peuget et al. [34] also observed an upward shift in wave number of the Raman band situated at about 480 cm^{-1} that could be interpreted as a decrease in the Si–O–Si angle [31,35]. Nevertheless it is necessary to specify that alpha disintegration or such ion irradiations induced at the same time nuclear and electronic energy interactions. So the structural modifications observed can not actually be ascribed to a specific type of interactions. Finally let us mention the atomistic modeling results obtained by Delaye, when studying the effect of nuclear interactions on the glass structure, who observed slight residual depolymerization after the passage of the recoil nucleus in the intermediate regions of displacement cascades where the projectile energy was not sufficient to ensure complete thermal relaxation [19].

5.3. Interpretation of the evolutions observed

This discussion of the structural origin of variations in nuclear glass macroscopic properties under irradiation must also be considered in terms of the

idea of a hypothetical increase in the glass fictive temperature caused by irradiation, as postulated by Simon [28], Galeener [36], Geissgerber [37] and Devine [31] to account for the evolution of amorphous silica under irradiation. Local disorganization of the glass equivalent to a significant temperature rise is observed during each displacement cascade. The material then remains in this condition after the passage of the projectile because of insufficient thermal relaxation [31]. All traces of the initial structure are thus lost, and the residual glass structure resembles a glass quenched at high temperature. According to this hypothesis, the accumulation of isolated events throughout the glass volume results in a totally damaged material; in Marples' model this corresponds to a density change proportional to the damaged volume fraction. Saturation of the evolution of the macroscopic properties is thus observed when the entire glass volume is damaged.

The hypothetical glass fictive temperature rise is further corroborated by the fact that the density, modulus of elasticity and hardness of borosilicate glass diminish at high temperatures or according to the cooling rate in the same way as nuclear glasses under irradiation [38–42]. A very interesting parallel can be drawn with the numerical modeling work done by Ito and Taniguchi [43,44] on the effect of the temperature and cooling rate on the structure and mechanical behavior of an aluminosilicate glass. Quenched glass has a lower Young's modulus and flows more readily than annealed glass; this difference is qualitatively in agreement with the behavior observed under the effect of alpha decay in R7T7-type glass. The structural analysis of quenched and annealed glass by Ito and Taniguchi [43,44] shows a change in the ring size distribution and in particular an increase in the number of small rings, together with a decrease of about 3° in the mean Si–O–Si angle. Moreover, the quenched glass structure is less polymerized than the annealed glass; this accounts for the lower modulus of elasticity and facilitates plastic deformation mechanisms. The changes in the reported mechanical properties and structure between annealed and quenched glass are thus qualitatively in agreement with the behavior observed following irradiation in nuclear glasses.

6. Conclusion

The behavior of nuclear glasses under alpha self-irradiation was investigated by characterizing the properties of four glass samples doped with 0.04, 0.4, 1.2 and 3.25 wt% $^{244}CmO_2$ as a function of the cumulative alpha decay up to about 3×10^{18} α/g, corresponding to several thousand years of storage of the current industrial glass. An alpha decay dose of this magnitude does not cause any variation in the initial alteration rate exceeding the measurement uncertainty, which means that the chemical reactivity of the glass with pure water is not affected by such levels of alpha doses. Slight glass swelling (about 0.5%) was observed together with an appreciable improvement in its mechanical properties, i.e. a 30% hardness reduction and increased resistance to cracking. These changes were observed for doses ranging from 10^{17} α/g to 2×10^{18} α/g. No further significant variation was observed at higher doses.

The experimental data do not reveal any dose rate effect within the range covered by the four glass compositions studied at room temperature. Comparing the experimental data with other findings obtained by atomistic modeling and external irradiation suggests that nuclear interactions caused by alpha decay recoil nuclei could be responsible for the experimental variations observed. These modifications could be described using a local quenching model along the path of the recoil nuclei, resulting in structure with a higher fictive temperature. The slightly lower degree of polymerization would account for the observed changes in its macroscopic properties. Finally, considering the loss of any trace of the initial state after the passage of the recoil nucleus, a simple damage recovery model of the damage zones describes the evolution of the properties versus the dose. In this case, the macroscopic properties stabilize when all the material has been damaged, suggesting that in the absence of another structural change mechanism the properties should remain constant at alpha doses greatest than 3×10^{18} α/g.

Characterization of the macroscopic behavior of doped glass will continue in the future to confirm the stabilization of the macroscopic properties as a function of the alpha dose. Specific experiments are now in progress to acquire structural data on irradiated glass in order to better describe nuclear glass behavior under irradiation.

Acknowledgements

This study was carried out under a research program funded jointly by the CEAand COGEMA. The authors are grateful to the DHA technicians

for fabricating and characterizing the materials, to the Atalante staff for their technical support, and to the COGEMA Marcoule central analysis laboratory for chemical composition analysis of the curium-doped glass.

References

[1] J.E. Mendel, W.A. Ross, F.P. Roberts, R.P. Turcotte, Y.B. Katayama, J.H. Westik, in: Proceedings of the Symposium on the Management of Radioactive Waste from Nuclear Fuel Cycle, Vienna, vol. 2, 1976, p. 49.
[2] R.P. Turcotte, F.P. Roberts, Phase behavior and radiation effects in high level waste glass, BNWL-SA-6168, 1977.
[3] F.P. Roberts, Irradiation effects on borosilicate waste glasses, PNL-SA-8182, 1980.
[4] N.E. Bibler, in: S.V. Topp (Ed.), Scientific Basis for Nuclear Waste Management, 1981, p. 681.
[5] J.A.C. Marples, Nucl. Instrum. and Meth. B 32 (1988) 480.
[6] Hj. Matzke, E. Vernaz, J. Nucl. Mater. 201 (1993) 295.
[7] T. Banba, S. Matsumoto, S. Murakoa, K. Yamada, M. Saito, H. Ishikawa, N. Sasaki, Mater. Res. Soc. Symp. Proc. 353 (1995) 1397.
[8] Y. Inagaki, H. Furuya, K. Idemitsu, T. Banba, S. Matsumoto, S. Murakoa, Mater. Res. Soc. Symp. Proc. 257 (1992) 199.
[9] Y. Inagaki, H. Furuya, Y. Ono, K. Idemitsu, T. Banba, S. Matsumoto, S. Murakoa, Mater. Res. Soc. Symp. Proc. 294 (1993) 191.
[10] W.J. Weber, F.P. Roberts, Nucl. Tech. 60 (1983) 178.
[11] R.C. Ewing, W.J. Weber, F.W. Clinard, Progr. Nucl. Energy 29 (1995) 63.
[12] W.J. Weber, R.C. Ewing, C.A. Angell, G.W. Arnold, A.N. Cormack, J.M. Delaye, D.L. Griscom, L.W. Hobbs, A. Navrotsky, D.L. Price, A.M. Stoneham, M.C. Weinberg, J. Mater. Res. 12 (1997) 1946.
[13] C. Lopez, PhD thesis, University of Paris XI, 2002.
[14] J.-N. Cachia, X. Deschanels, T. Charpentier, D. Sakellariou, C. Den Auwer, J. Phalippou, in: Advances in Actinides Science, Royal Society of Chemistry, submitted for publication.
[15] D.M. Wellman, J.P. Icenhower, W.J. Weber, J. Nucl. Mater. 340 (2005) 149.
[16] S. Peuget, P. Nivet, J. Ducros, J.M. Bart, J.L. Loubet, S. Pavan, in Proceedings of the Twentieth International Congress on Glass, Kyoto, O-07-023, 2004.
[17] S. Peuget, P.-Y. Noel, J.L. Loubet, S. Pavan, P. Nivet, J. Ducros, Nucl. Instrum. and Meth. In Phys. Res., accepted for publication.
[18] Hj. Matzke, in: CEA/Valrhô Summer Session Proceedings on Glass: Scientific Research for High Performance Containment, Méjannes-Le-Clap, 1997, p. 149.
[19] J.M. Delaye, D. Ghaleb, Phys. Rev. B 71 (2005) 224203, 224204.
[20] P. Cheminant-Coatanlem, Étude du comportement sous irradiation neutronique du diborure de hafnium, PhD thesis, Université Paris-Sud, 1997.
[21] S. Sato et al., Nucl. Mater. 152 (1988) 265.
[22] R.P. Turcotte, Radiation effects in solidified high-level wastes, part 2 – Helium behaviour, BNWL-2051, 1976.
[23] G. Malow, H. Andersen, Scientific Basis for Nuclear Waste Management 1 (1979) 109.
[24] B.R. Lawn, D.B. Marshall, J. Am. Ceram. Soc. 62 (1979) 347.
[25] S. Peuget, C. Jégou, V. Broudic, D. Roudil, X. Deschanels, J.M. Bart, Mater. Res. Soc. Symp. Proc. 824 (2004) 315.
[26] S. Ito, J. Ceram. Soc. Jap. 112 (2004) 477.
[27] N. Jacquet-Francillon, Les verres dans les stockages, CEA internal report R-5656, 1994.
[28] I. Simon, J. Am. Ceram. Soc. 40 (1957) 150.
[29] W. Primak, Phys. Rev. 110 (1958) 1240.
[30] J.B. Bates, R.W. Hendricks, L.B. Schaffer, J. Chem. Phys. 61 (1974) 4167.
[31] R.A.B. Devine, Nucl. Instrum. and Meth. B 91 (1994) 378.
[32] B. Boizot, S. Agnello, B. Reynard, R. Boscaino, G. Petite, J. Non-Cryst. Solids 235 (2003) 22.
[33] N.J. Hess, W.J. Weber, S.D. Conradson, J. Nucl. Mater. 254 (1998) 175.
[34] S. Peuget, P.-Y. Noel, J. de Bonfils, G. Panczer, A. Chenet, J. Non-Cryst. Solids., submitted for publication.
[35] B. Boizot, G. Petite, D. Ghaleb, B. Reynard, G. Calas, J. Non-Cryst. Solids 243 (1999) 268.
[36] F.L. Galeener, in: P.H. Gaskell, A.E. Davis, J.N. Parker (Eds.), The Structure of Non-Crystalline Materials II, 1983, p. 337.
[37] A.E. Geissberger, F.L. Galeener, Phys. Rev. B 28 (1983) 3266.
[38] H. Scholze, Le verre – Nature, structure et propriétés, Deuxième édition, Institut du verre, 1980.
[39] W.H. Otto, J. Am. Ceram. Soc. 44 (1961) 68.
[40] P.K. Gupta, M.L. Lui, P.J. Bray, J. Am. Ceram. Soc. 68 (1985) C-82.
[41] H. Li, A. Agarwal, M. Tomozawa, J. Am. Ceram. Soc. 78 (1995) 1393.
[42] B. Varughese, Y.K. Lee, M. Tomozawa, J. Non-Cryst. Solids 241 (1998) 134.
[43] S. Ito, T. Taniguchi, J. Non-Cryst. Solids 349 (2004) 173.
[44] T. Taniguchi, S. Ito, Phys. Chem. Glasses 43C (2003) 493.